



Regularized Laplacian Zero Crossings as Optimal Edge Integrators

R. KIMMEL AND A.M. BRUCKSTEIN

Department of Computer Science, Technion–Israel Institute of Technology, Technion City, Haifa 32000, Israel

Received September 12, 2001; Revised January 8, 2002; Accepted January 9, 2003

Abstract. We view the fundamental edge integration problem for object segmentation in a geometric variational framework. First we show that the classical zero-crossings of the image Laplacian edge detector as suggested by Marr and Hildreth, inherently provides optimal edge-integration with regard to a very natural geometric functional. This functional accumulates the inner product between the normal to the edge and the gray level image-gradient along the edge. We use this observation to derive new and highly accurate active contours based on this functional and regularized by previously proposed geodesic active contour geometric variational models. We also incorporate a 2D geometric variational explanation to the Haralick edge detector into the geometric active contour framework.

Keywords: edge detection, active contours, segmentation, calculus of variations, level sets

1. Introduction

Edge integration for segmentation is an old, yet still very active area of research in low-level image analysis. Textbooks in computer vision treat edge detection and edge integration as separate topics, the first being considered one of labelling edges in the image to be followed by a process of integrating the local “edges” into meaningful curves. In fact, one may view basic edge detection as a process of estimating the gradient of the image, i.e. computing at each pixel (x, y) the values $u(x, y) \triangleq \frac{\partial}{\partial x} I(x, y)$ and $v(x, y) \triangleq \frac{\partial}{\partial y} I(x, y)$ by using the values of $I(x, y)$ over a neighborhood $\mathcal{N}(x, y)$ of (x, y) and designating as edges the places where the length of the gradient vector estimate $[u, v] = (\nabla I)$ exceeds some threshold value.

The more advanced edge detectors such as those proposed by Marr and Hildreth (1980) attempt to locate points or curves defined by local maxima of the image gradient. The Marr Hildreth proposal for edge detection yields curves that delineate the zero crossing of the Laplacian operator applied to a smoothed version of the image input. The smoothing proposed is via a Gaussian convolution operator and its width is a parameter that can be varied providing the opportunity

to do scale space processing and “vertical” integration on the zero-crossing curves. Improvements of the zero crossing of the Laplacian operator such as those proposed by Haralick (1984) and popularized by Canny (1986) attempt to locate points or curves defined as local maxima of the gradient magnitude along the gradient direction. Similar analytically yet more accurate numerically is the zero crossing of the second derivative of the intensity along the gradient direction (Haralick, 1984; Deriche, 1987).

In this paper we propose to regard the edge detection and integration process as a way to determine curves in the image plane that pass through points where the gradient is high and whose direction best corresponds to the local edge direction predicted by the estimated gradient. Indeed, if we somehow estimate the gradient field $[u(x, y), v(x, y)]$ based on considering $I(x, y)$ for each pixel (x, y) over some neighborhood $\mathcal{N}_\sigma(x, y)$, where σ is a size parameter, we shall have at each point a value, given by the intensity of the gradient $(u^2(x, y) + v^2(x, y))^{\frac{1}{2}}$, that tells us how likely an edge is at this point and, if an edge exists, its likely direction will be perpendicular to the vector $[u(x, y), v(x, y)]$. It is therefore natural to look for curves in the image plane, $C(s) = [x(s), y(s)]$, that pass through points

with high intensity gradients with tangents agreeing as much as possible to the edge directions there (in this paper s denotes the arclength parameterization). Thus we are led to consider the following functional, evaluating the quality of $C(s)$ as an edge-curve candidate,

$$\psi_\rho(C(s)) = \int_0^L \rho \left([u(C(s)), v(C(s))] \cdot \begin{bmatrix} 0 & 1 \\ -1 & 0 \end{bmatrix} \left[\frac{dC(s)}{ds} \right]^T \right) ds \quad (1)$$

where $\rho(\cdot)$ can be a some convex symmetric scalar function that satisfies $\rho'(0) = 0$, and $\rho'' > 0$. Other less restrictive requirements can also be considered and in this paper we first take the identity $\rho(\alpha) = \alpha$ which is sensitive to gray scale inversion. We will refer to insensitivity to gray scale inversion as inverse intensity invariance property. For this property to hold, it is easy to see that ρ needs to be a symmetric ($\rho(\alpha) = \rho(-\alpha)$) function. As an example we will consider a 'robust' version where $\rho(\alpha) = |\alpha|$.

Here, the inner product of $\nabla I = [u, v]$ with the normal to $C(s)$, given by

$$\vec{n}(s) = \begin{bmatrix} 0 & 1 \\ -1 & 0 \end{bmatrix} \left[\frac{dC(s)}{ds} \right]^T, \quad (2)$$

where $C(s)$ is an arclength parameterized curve, is a measure of how well $C(s)$ is locally tracking an edge. Indeed, we want $C(s)$ to pass at high gradient locations in the edge direction, and hence the inner product of its normal with the estimated gradient of I should be high, indicating both alignment and considerable change in image intensity there. This inner product will also be proportional to the gradient magnitude, since

$$[u(C(s)), v(C(s))] \begin{bmatrix} 0 & 1 \\ -1 & 0 \end{bmatrix} \left[\frac{dC}{ds} \right]^T = |\nabla I| \cdot \cos(\theta), \quad (3)$$

where θ is the angle between the outward pointing normal \vec{n} to $C(s)$ and the gradient direction.

The functionals ψ_ρ measure how well an arclength parameterized curve of length L approximates an edge in the image plane. Our task, of course is to determine several most probable edge curves in the image plane. We shall do so by determining curves that locally maximize these functionals.

Suppose first that we are considering closed contours $C(s)$, and that $\rho(\alpha) = \alpha$. Then, we have that

$$\psi(C(s)) = \oint_{C(s)} \left(u(C(s)) \frac{d}{ds} y(s) - v(C(s)) \frac{d}{ds} x(s) \right) ds, \quad (4)$$

and Green's theorem yields

$$\psi(C(s)) = \iint_{\Omega_C} \left(\frac{\partial}{\partial y} v(x, y) + \frac{\partial}{\partial x} u(x, y) \right) dx dy, \quad (5)$$

where Ω_C is the region inside $C(s)$. But, recalling that $v(x, y)$ is an estimate of $\frac{\partial}{\partial y} I(x, y)$ and $u(x, y)$ an estimate of $\frac{\partial}{\partial x} I(x, y)$, we have

$$\begin{aligned} \psi(C(s)) &\cong \iint_{\Omega_C} \left(\frac{\partial^2}{\partial x^2} I(x, y) + \frac{\partial^2}{\partial y^2} I(x, y) \right) dx dy \\ &\cong \iint_{\Omega_C} (\Delta I(x, y)) dx dy. \end{aligned} \quad (6)$$

Therefore, the functional that we want to maximize is the integrated Laplacian over the area enclosed by $C(s)$. This means that if we have an area where the Laplacian is positive, $\psi(C(s))$ should expand from within this area to the places where $\Delta I(x, y)$ becomes zero and subsequently changes sign. This shows that optimal edge-curves in the sense of maximizing $\psi(C(s))$ are the zero crossings of the Laplacian. If we initialize $C(s)$ as a small circular "bubble" at a place where $\Delta I(x, y)$ is positive and then let $C(s)$ evolve according to a rule that implements a gradient descent in conjunction with the functional $\psi(C(s))$, i.e. we implement

$$\frac{d}{dt} C(s, t) = \frac{\delta \psi(C(s; t))}{\delta C}, \quad (7)$$

the curve $C(s, t)$ will expand in time t to the nearest zero-crossing curve of the input image Laplacian. Note that in case of homogeneous regions or very noisy images, this process will either be stuck at the initialization curve or will yield a myriad of little islands corresponding to false edge contours, so extra care should be taken in these cases.

So far, we have obtained a beautiful interpretation of the classical Marr-Hildreth edge detection method (Marr and Hildreth, 1980). The zero-crossings of the Laplacian are curves that best integrate the edges, in the sense of our functional $\psi_\rho(C(s))$ with $\rho(\alpha) = \alpha$, if

we wish to do so based on gradients estimated for the (smoothed) input image $I(x, y)$. While this fact is pedagogically very pleasing, it does not alleviate the notorious over sensitivity properties of this edge-detector which in noisy images yields lots of false edge curves. However, we shall show here that this insight provides the basis for a class of new and practical active contour processes which enhance and improve upon previously designed such methods for image segmentation.

The importance of using directional information for delicate segmentation tasks was recently also realized by Vasilevskiy and Siddiqi (2001) in a related result. They used alignment with a general vector field as minimization criteria for segmentation of complicated closed thin structures in 3D medical images.

An interesting question is how to relate our method to the Haralick (1984) edge detector, used as a main ingredient in the Canny (1986) edge operator. The question here is: what is the variational approach that gives a geometric explanation to the Canny or Haralick edge detection operator.

In the next section we give a 2D geometric variational explanation to the Haralick-Canny-type edge detector. We show that the Haralick-Canny operator uses a topological homogeneity measure that regularizes the above alignment term, as we first presented in Kimmel and Bruckstein (2002). When used as part of an active contour model, the quality of the edges captured by active contours is somewhat better when using the GAC as a regularization term for the alignment based functional rather than the Haralick-Canny topological homogeneity term. Then, we extend our results from Kimmel and Bruckstein (2001), and present the full derivation of the variational results leading to the new edge integration processes. Finally, we show the performance of the resulting algorithms.

2. Haralick-Canny-Type Edge Detectors

An interesting question is how to relate the proposed method to the Haralick (1984) edge detector, used as a main ingredient in the Canny (1986) edge operator. The question here is: what is the variational approach that gives a geometric explanation to the Canny or Haralick edge detection operator. Recently, we have found an interesting answer to this question. The quality of the edges captured by active contours is somewhat better when using the GAC as a regularization term for the alignment based functional, while the Haralick-Canny operator can be shown to use a topological

homogeneity measure that regularizes the alignment term, as shown in Kimmel and Bruckstein (2002).

As in Marr-Hildreth edge detectors, some smoothing of the image is performed first; then the Haralick edge detector (Haralick, 1984; Canny, 1986; Deriche, 1987) is defined by the zero crossings of the second derivative along the image gradient direction. Given the gray level image $I(x, y) : \mathbb{R}^2 \rightarrow [0, 1]$, define the gradient direction vector field

$$\vec{\xi}(x, y) = \frac{\nabla I}{|\nabla I|} = \frac{\{I_x, I_y\}}{|\nabla I|},$$

and the corresponding orthogonal vector field,

$$\vec{\eta}(x, y) = \frac{\bar{\nabla} I}{|\nabla I|} = \frac{\{-I_y, I_x\}}{|\nabla I|},$$

so that $\langle \vec{\eta}, \vec{\xi} \rangle = 0$ (see Fig. 1).

The Haralick edge detector outlines the image locations where both $|\nabla I|$ is larger than some threshold and $I_{\xi\xi} = 0$. This procedure was indeed observed to yield better results compared to the zero crossings of the Laplacian. We will not review here the justifications provided before for this edge detection process, yet, to the best of our knowledge there exist no rigorous explanations or analysis for this operator in two dimensions. The improved results obtained with the Haralick edge detector were explained, as we stated before, based on one dimensional arguments.

Let us try to justify the good properties of the Haralick-Canny-edges from a variational point of view. We formulate the edge operator as a result of a variational principle in 2D and in the process we get a better understanding and a rigorous mathematical meaning for the Haralick edge tracing operator. First, we use the rotation invariance property of the Laplacian to define

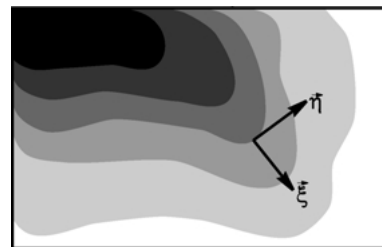


Figure 1. The level sets of I , and $\{\vec{\xi}, \vec{\eta}\}$, the gradient and the orthogonal directions.

the operator

$$I_{\xi\xi} = I_{\xi\xi} + I_{\eta\eta} - I_{\eta\eta} = \Delta I - I_{\eta\eta}$$

$$= \frac{I_x^2 I_{xx} + 2I_x I_y I_{xy} + I_y^2 I_{yy}}{I_x^2 + I_y^2}.$$

The edge detector provides curves along which $\Delta I - I_{\eta\eta} = 0$. We have shown in the introduction that $\Delta I \vec{n} = 0$ is the result of maximizing the geometric integral measure

$$\oint_0^L \langle \nabla I, \vec{n} \rangle ds, \tag{8}$$

where s is the arclength parameter of the curve, \vec{n} its normal, and L its total length. Let us define, as usual, \vec{n} , κ , and \vec{t} to be the unit normal, the curvature, and the tangent of the curve C , respectively. We have that $\kappa \vec{n} = C_{ss}$, and $\vec{t} = C_s = C_p / |C_p|$. Let Ω_C be the domain inside the curve C , see Fig. 2.

The alignment measure (8) should be modified to handle similarly hills and dips. Towards that goal, we first define a unit vector field $\vec{v}(x, y) : \Omega \rightarrow S^1$ such that

$$\vec{v}(x, y) = \begin{cases} \vec{\xi}(x, y) & \text{the level set interior is increasing} \\ -\vec{\xi}(x, y) & \text{the level set interior is decreasing} \end{cases}.$$

Note that \vec{v} can be easily computed from the image.

Next, consider the alignment measure

$$\oint_0^L \text{sign}(\langle \vec{v}, \nabla I \rangle) \langle \nabla I, \vec{n} \rangle ds. \tag{9}$$

Here the term $\text{sign}(\langle \vec{v}, \nabla I \rangle)$ verifies that the modified normal of the curve, given by $\text{sign}(\langle \vec{v}, \nabla I \rangle) \vec{n}$, is oriented uphill for all hills, and downhill for all the dips in the image. Note that the normal orientation is smooth almost everywhere along the curve, if we exclude pathological cases in which our curve tracks a level set passing through a saddle point in the image. The Euler-Lagrange equation corresponding to (9) is given by $\text{sign}(\langle \vec{v}, \nabla I \rangle) \Delta I = 0$.

The quantity $I_{\eta\eta}$ is known to be the curvature of the image level set, multiplied by the image gradient magnitude, that is,

$$I_{\eta\eta} = |\nabla I| \text{div} \left(\frac{\nabla I}{|\nabla I|} \right) = \kappa_I |\nabla I|,$$

where κ_I is the curvature of the image level sets. In order to understand the meaning of the Haralick operator, we search for a geometric functional defined along a curve that yields $I_{\xi\xi} \vec{n} = 0$ as an Euler Lagrange equation. Toward this goal, we may equivalently search for the geometric functional along a curve that yields $(\Delta I - I_{\eta\eta}) \vec{n} = 0$ as an Euler Lagrange equation. Consider the general scalar cost function

$$\iint_{\Omega_C} g(x, y) dx dy,$$

that integrates the cost function g inside the curve C . Then, by Green's theorem, the corresponding EL equation is given by $g(C) \vec{n} = 0$, see for example (Zhu et al., 1995; Paragios and Deriche, 2000) Hence if we set, $g(x, y) = I_{\eta\eta}$, we can get closer to the required result. That is, we will try to find a geometric meaning for $\iint_{\Omega_C} I_{\eta\eta} dx dy$.

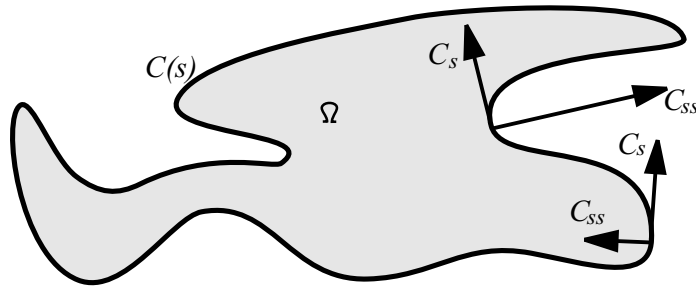


Figure 2. A closed curve C , with C_s the unit tangent, $\kappa \vec{n} = C_{ss}$ the curvature vector, and Ω_C the area inside the curve.

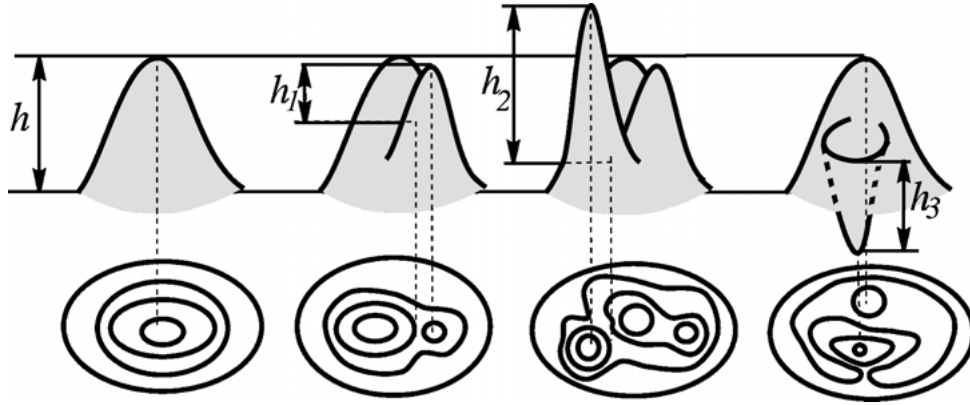


Figure 3. Integration of $I_{\eta\eta}$ in closed contours for various image surfaces. The integration results left to right are: $2\pi h$, $2\pi(h + h_1)$, $2\pi(h + h_1 + h_2)$, and $2\pi(h - h_3)$.

We look into the geometric interpretation of the second part in the Haralick operator

$$\begin{aligned} \iint_{\Omega_C} I_{\eta\eta} dx dy &= \iint_{\Omega_C} \kappa_I |\nabla I| dx dy \\ &= \int_{\mathbb{R}} \left(\int_{I^{-1}(u) \cap \Omega_C} \kappa_I ds \right) du, \end{aligned}$$

where we used the co-area equation (Evans and Gariepy, 1992) to change coordinates from $dx dy$ to $ds du$, where $u = I(x, y)$. Here s is the arclength of the image level sets, and u represents its gray values. For a closed (level set) contour we have that $\oint \kappa_I ds = 2\pi$. Figure 3 shows the result of integration over $I_{\eta\eta}$ in a closed contour for various simple image surfaces. Therefore, the integral over $I_{\eta\eta}$ inside C somehow measures the topological uniformity of I in Ω_C . We see that this is a measure generalizing the 1D total variation and is a function of the topological-complexity of I over Ω_C .

If we look more carefully at the measure $\iint_{\Omega_C} I_{\eta\eta} dx dy$, we see, as in the right case of Fig. 3, that valleys or dips contribute a negative value to the total cost. This contradicts what would have been expected from a proper topological complexity measure. A simple modification however can cure this drawback.

Let us redefine the topological complexity measure to be

$$\iint_{\Omega_C} \text{sign}(\langle \vec{v}, \vec{\xi} \rangle) I_{\eta\eta} dx dy,$$

which gives a positive sign to all topological parts inside the contour C . This now becomes a proper topo-

logical complexity measure of the interior with equal contribution of ‘hills’ and ‘dips’.

We can therefore combine these two measures into one that is given by

$$\begin{aligned} \psi_H(C) &= \oint_C \text{sign}(\langle \vec{v}, \vec{\xi} \rangle) \langle \nabla I, \vec{n} \rangle ds \\ &\quad - \iint_{\Omega_C} \text{sign}(\langle \vec{v}, \vec{\xi} \rangle) I_{\eta\eta} dx dy \\ &= \iint_{\Omega_C} \text{sign}(\langle \vec{v}, \vec{\xi} \rangle) (\Delta I - I_{\eta\eta}) dx dy \\ &= \iint_{\Omega_C} \text{sign}(\langle \vec{v}, \vec{\xi} \rangle) I_{\xi\xi} dx dy. \end{aligned} \quad (10)$$

This measure yields, as expected, the EL equation

$$\text{sign}(\langle \vec{v}, \vec{\xi} \rangle) I_{\xi\xi} = 0,$$

or in its simpler edge detector form $I_{\xi\xi} = 0$.

Combining the above derivations into a unified framework, we have that the Haralick operator searches for alignment of the edge normals with the image gradients, while also minimizing a “topological uniformity” or “total variation like” measure inside the contour. The only difference between the Marr-Hildreth Laplacian zero crossings operator (Marr and Hildreth, 1980; Marr, 1982) and the Haralick operator (Haralick, 1984; Canny, 1986; Deriche, 1987), is the additional minimization term measuring the topological complexity inside the outlined edge contour. This extra term prefers to group together uniform areas, avoiding noisy regions, and thereby has the chance to yield more robust edge curves for better object segmentation.

The uniformity measure expressed by $\iint_{\Omega_C} \text{sign}(\langle \vec{v}, \vec{\xi} \rangle) I_{\eta\eta} dx dy$ is just one possible choice that may be appropriate in the context of edge detection and integration problems. We could add to our geometric measure other useful terms. Probably the simplest example could be based on incorporating some knowledge on the gray levels of objects expected to appear in a scene. For example, if we know that the objects we try to segment are expected to have a constant gray level c_1 , and the background is expected to be c_2 , then the functional we could add to the cost function may be defined by

$$\begin{aligned} \psi_H(C) = & \int_{\partial\Omega_C} \text{sign}(\langle \vec{v}, \vec{\xi} \rangle) \langle \nabla I, \vec{n} \rangle ds \\ & - \iint_{\Omega_C} \text{sign}(\langle \vec{v}, \vec{\xi} \rangle) \kappa_I |\nabla I| dx dy \\ & - \alpha \left(\iint_{\Omega_C} (I - c_1)^2 dx dy \right. \\ & \left. + \iint_{\Omega \setminus \Omega_C} (I - c_2)^2 dx dy \right), \end{aligned}$$

where Ω_C defines the regions inside our ‘objects’, and $\Omega \setminus \Omega_C$ defines the background region. As Euler-Lagrange equations we then get the edge detector operator

$$\begin{aligned} & \left(\text{sign}(\langle \vec{v}, \vec{\xi} \rangle) (\Delta I - I_{\eta\eta}) + 2\alpha(c_2 - c_1) \right. \\ & \left. \times \left(I - \frac{c_1 + c_2}{2} \right) \right) \vec{n} = 0, \end{aligned}$$

which is a trade-off between gradient alignment coupled with topological uniformity, and the simplest segmentation we can think of: gray level thresholding!

Next, we introduce some dynamics to our edge detectors so that edges can be smoothly tailored and integrated into meaningful boundaries of objects. For that we develop an active contour model that incorporates both alignment terms as well as classical integral geometric measures and expected gray-level priors.

3. Closed Active Contours: Derivation

Motivated by the classical ‘snakes’ (Kass et al., 1988), non-variational geometric active contours (Malladi et al., 1993; Caselles et al., 1993; Malladi et al., 1995),

and finally by the ‘geodesic active contours’ (Caselles et al., 1997), we search for simple parametric curves in the plane that map their arclength interval $[0, L]$ to the plane, such that $C : [0, L] \rightarrow \mathbb{R}^2$, or in an explicit parametric form $C(s) = [x(s), y(s)]$, that maximize one of the integral geometric measures $\psi(C)$. As we stated before, s is the arclength parameter, hence we have the relation between the arclength s and a general arbitrary parameterization p , given by

$$ds = \sqrt{\left(\frac{dx(p)}{dp}\right)^2 + \left(\frac{dy(p)}{dp}\right)^2} dp = |C_p| dp. \quad (11)$$

We define, as usual, \vec{n} , κ , and \vec{t} to be the unit normal, the curvature, and the tangent of the curve C . We have that $\kappa \vec{n} = C_{ss}$, and $\vec{t} = C_s = C_p / |C_p|$. We first consider the geometric functional

$$\psi_\rho(C) = \oint_0^L \rho(\langle \vec{V}, \vec{n} \rangle) ds. \quad (12)$$

This is an integration along the curve C of a function ρ defined in terms of a vector field $\vec{V} = [u(x, y), v(x, y)]$, where for example we can take $\vec{V} = \nabla I(x, y) = [I_x, I_y]$ as the gray level image gradient. Our goal is to find curves C that minimize the above geometric functional.

In a general parametric form, we have the following re-parameterization invariant measure

$$\psi_\rho(C) = \oint_0^1 \rho(\langle \vec{V}, \vec{n} \rangle) |C_p| dp. \quad (13)$$

Define, $\alpha \equiv \langle \vec{V}, \vec{n} \rangle$. The Euler Lagrange (EL) equations $\delta\psi_\rho(C)/\delta C = 0$ should hold along the extremum curves, and for a closed curve these equations are

$$\frac{\delta\psi_\rho(C)}{\delta C} = \left(\begin{array}{cc} \frac{\partial}{\partial x} - \frac{d}{dp} \frac{\partial}{\partial x_p} \\ \frac{\partial}{\partial y} - \frac{d}{dp} \frac{\partial}{\partial y_p} \end{array} \right) \rho(\alpha) |C_p|, \quad (14)$$

or in a more compact form

$$\frac{\delta\psi_\rho(C)}{\delta C} = \left(\frac{\partial}{\partial C} - \frac{d}{dp} \frac{\partial}{\partial C_p} \right) \rho(\alpha) |C_p|, \quad (15)$$

where we use the shorthand notation $\partial/\partial C = [\partial/\partial x, \partial/\partial y]^T$ and $\partial/\partial C_p = [\partial/\partial x_p, \partial/\partial y_p]^T$. In case of an open curve, one must also consider the end

points and add additional constraints to determine their optimal locations.

Before we work out the general $\rho(\alpha)$ case let us return to the simple example discussed in the introduction, where $\rho(\alpha) = \alpha$. In this case we have that

$$\begin{aligned}\psi(C) &= \oint_0^1 \langle \vec{V}, \vec{n} \rangle |C_p| dp \\ &= \oint_0^1 \left\langle \vec{V}, \frac{[-y_p, x_p]}{|C_p|} \right\rangle |C_p| dp \\ &= \oint_0^1 (-y_p u + x_p v) dp.\end{aligned}\quad (16)$$

The EL equation for the x part is given by

$$\begin{aligned}\frac{\delta\psi}{\delta x} &= \left(\frac{\partial}{\partial x} - \frac{d}{dp} \frac{\partial}{\partial x_p} \right) (-y_p u + x_p v) \\ &= -y_p u_x + x_p v_x - \frac{d}{dp} v \\ &= -y_p u_x + x_p v_x - v_x x_p - v_y y_p \\ &= -y_p (u_x + v_y) = -y_p \operatorname{div}(\vec{V}).\end{aligned}\quad (17)$$

In a similar way, the y part of the EL equations is given by

$$\begin{aligned}\frac{\delta\psi}{\delta y} &= \left(\frac{\partial}{\partial y} - \frac{d}{dp} \frac{\partial}{\partial y_p} \right) (-y_p u + x_p v) \\ &= -y_p u_y + x_p v_y + \frac{d}{dp} u \\ &= -y_p u_y + x_p v_y + u_x x_p + u_y y_p \\ &= x_p (u_x + v_y) = x_p \operatorname{div}(\vec{V}).\end{aligned}\quad (18)$$

Since the EL equations are derived with respect to a geometric measure, we can use the freedom of reparameterization for the curve C , divide by $|C_p|$, and obtain the “geometric EL equation:” $\delta\psi/\delta C = \operatorname{div}(\vec{V})\vec{n}$, and for $\vec{V} = \nabla I(x, y)$ we have $\delta\psi/\delta C = \Delta I \vec{n}$, where $\Delta I \equiv I_{xx} + I_{yy}$ is the usual Laplacian operator. It is obvious from this that the geometric EL condition is satisfied along the zero crossing curves of the image Laplacian, which, as described above, nicely explains the Marr and Hildreth (1980) and Marr (1982) edge detector from a global-variational point of view. Below, we shall extract further insights and segmentation schemes from this observation. We note that heuristic and non-variational flows on vector fields were presented in Xu and Prince (1998) and Paragios et al. (2001).

As a second example we consider $\rho(\alpha) = |\alpha| = \sqrt{\alpha^2}$. The EL equation in this case is given by

$$\begin{aligned}\frac{\delta\psi}{\delta C} &= \frac{\langle \vec{V}, \vec{n} \rangle}{|\langle \vec{V}, \vec{n} \rangle|} \operatorname{div}(\vec{V})\vec{n} \\ &= \operatorname{sign}(\langle \vec{V}, \vec{n} \rangle) \operatorname{div}(\vec{V})\vec{n},\end{aligned}\quad (19)$$

and for $\vec{V} = \nabla I$ we have $\delta\psi/\delta C = \operatorname{sign}(\langle \nabla I, \vec{n} \rangle) \Delta I \vec{n}$. The additional term $\operatorname{sign}(\langle \nabla I, \vec{n} \rangle)$, allows the gradient descent flow $C_t = \delta\psi/\delta C$, to automatically handle changing contrasts between the objects and the background. Hence, it handles equally well an image of dark objects on bright background and the negative of this image.

Now, we are ready to pursue the general case for $\rho(\alpha)$ in the functional $\psi_\rho(C)$ (where $\alpha = \langle \vec{V}, \vec{n} \rangle$). We shall often use the following, readily verified, relationships:

$$\begin{aligned}\frac{d}{dp} &= |C_p| \frac{d}{ds} \\ \frac{\partial |C_p|}{\partial C_p} &= \vec{t} \\ \frac{d\vec{n}}{ds} &= -\kappa \vec{t} \\ \frac{d\vec{t}}{ds} &= \kappa \vec{n} \\ \frac{d\rho(\alpha)}{ds} &= \rho' \alpha_s = \langle \nabla \rho, \vec{t} \rangle \\ \frac{d\alpha}{ds} &= \langle \vec{V}_s, \vec{n} \rangle + \langle \vec{V}, \vec{n}_s \rangle = \langle \vec{V}_s, \vec{n} \rangle - \kappa \langle \vec{V}, \vec{t} \rangle \\ \frac{\partial \alpha}{\partial C_p} &= -|C_p|^{-1} \langle \vec{V}, \vec{t} \rangle \vec{n},\end{aligned}\quad (20)$$

and that

$$\left(\frac{\partial}{\partial C} - \frac{d}{dp} \frac{\partial}{\partial C_p} \right) (\alpha |C_p|) = |C_p| \operatorname{div}(\vec{V})\vec{n}.\quad (21)$$

Using these relations we have

$$\begin{aligned}\frac{\delta\psi_\rho(C)}{\delta C} &= \left(\frac{\partial}{\partial C} - \frac{d}{dp} \frac{\partial}{\partial C_p} \right) \rho(\alpha) |C_p| \\ &= \rho' \alpha_C |C_p| - \frac{d}{dp} (\rho' \alpha_C |C_p| + \rho \vec{t}) \\ &= \rho' \alpha_C |C_p| - \frac{d}{dp} (\rho' \alpha_C |C_p| + \rho' \alpha \vec{t} \\ &\quad - \rho' \alpha \vec{t} + \rho \vec{t}) \\ &= \rho' \alpha_C |C_p| - \frac{d}{dp} (\rho' \alpha_C |C_p| + \rho' \alpha \vec{t})\end{aligned}$$

$$\begin{aligned}
 & -\frac{d}{dp}(-\rho'\alpha\vec{t} + \rho\vec{t}) \\
 &= \rho'\alpha_C|C_p| - \rho'\frac{d}{dp}(\alpha_{C_p}|C_p| + \alpha\vec{t}) \\
 & \quad - \rho''\alpha_p(\alpha_{C_p}|C_p| + \alpha\vec{t}) - \frac{d}{dp}(-\rho'\alpha\vec{t} + \rho\vec{t}) \\
 &= \rho'|C_p|\operatorname{div}(\vec{V})\vec{n} - \rho''|C_p|\alpha_s(-\langle\vec{V}, \vec{t}\rangle\vec{n} + \alpha\vec{t}) \\
 & \quad - |C_p|\frac{d}{ds}(-\rho'\alpha\vec{t} + \rho\vec{t}) \\
 &= |C_p|(-\rho\kappa + \rho'(\operatorname{div}(\vec{V}) + \langle\vec{V}, \vec{n}\rangle\kappa) \\
 & \quad + \rho''(\langle\vec{V}_s, \vec{n}\rangle\langle\vec{V}, \vec{t}\rangle - \kappa\langle\vec{V}, \vec{t}\rangle^2))\vec{n} \\
 & \quad + \text{some additional tangential components.}
 \end{aligned} \tag{22}$$

Here we used the shorthand notations $\alpha_C = \nabla\alpha = [\alpha_x, \alpha_y]$, and $\alpha_{C_p} = \nabla_{C_p}\alpha$.

Note that by freedom of parameterization we have the first variation given by

$$\begin{aligned}
 \frac{\delta\psi_\rho(C)}{\delta C} &= (-\rho\kappa + \rho'(\operatorname{div}(\vec{V}) + \langle\vec{V}, \vec{n}\rangle\kappa) \\
 & \quad + \rho''(\langle\vec{V}_s, \vec{n}\rangle\langle\vec{V}, \vec{t}\rangle - \kappa\langle\vec{V}, \vec{t}\rangle^2))\vec{n} \\
 & \quad + \text{tangential components.}
 \end{aligned} \tag{23}$$

As a third example we add the additional topological homogeneity measure and consider again our geometric functional

$$\begin{aligned}
 \psi(C) &= \oint_0^L \operatorname{sign}(\langle\vec{v}, \vec{\xi}\rangle)\langle\nabla I(x, y), \vec{n}\rangle ds \\
 & \quad - \iint_{\Omega_C} \operatorname{sign}(\langle\vec{v}, \vec{\xi}\rangle)I_{\eta\eta} dx dy.
 \end{aligned} \tag{24}$$

As we have seen, the second term measures the topological uniformity inside the curve. Our goal is to find curves C that maximize the above geometric functional.

The Euler Lagrange (EL) equations $\delta\psi(C)/\delta C = 0$ should hold along the extremum curves, where $\delta\psi/\delta C = \operatorname{sign}(\langle\vec{v}, \vec{\xi}\rangle)(\Delta I - I_{\eta\eta})\vec{n}$. We could easily add terms to our functional, like the geodesic active contour model, to play the role of regularization. These terms could actually replace the topological-complexity measure with a simpler local implementation yielding better results especially if we couple it with the robust version.

3.1. Gradient Descent via Level Set Formulation

In order to determine optimal curves in the plane, we need to numerically solve the EL equations. Here we shall follow the ‘‘geodesic active contour philosophy,’’ see (Caselles et al., 1997), and design a curve evolution rule that is given by

$$C_t = \frac{\delta\psi_\rho(C)}{\delta C}. \tag{25}$$

This is a gradient descent rule with respect to the chosen cost functional, and in this flow one can consider only the normal components of $\delta\psi_\rho(C)/\delta C$, since tangential components have no effect on the geometry the propagating curve. Next, we can embed the curve in a higher dimensional $\phi(x, y)$ function, which implicitly represents the curve C as a zero set, i.e., $C = \{[x, y] : \phi(x, y) = 0\}$. In this way, the well known Osher and Sethian (1988) and Sethian (1996) level-set method can be employed to implement the propagation.

Given the curve evolution equation $C_t = \gamma\vec{n}$, its implicit level set evolution equation reads

$$\phi_t = \gamma|\nabla\phi|. \tag{26}$$

The equivalence of these two evolutions can be easily verified using the chain rule and the relation $\vec{n} = \nabla\phi/|\nabla\phi|$,

$$\begin{aligned}
 \phi_t &= \langle\nabla\phi, C_t\rangle = \langle\nabla\phi, \gamma\vec{n}\rangle \\
 &= \gamma\left\langle\nabla\phi, \frac{\nabla\phi}{|\nabla\phi|}\right\rangle = \gamma|\nabla\phi|.
 \end{aligned} \tag{27}$$

We readily have that

$$\begin{aligned}
 \vec{t} &= \frac{\bar{\nabla}\phi}{|\nabla\phi|} = \frac{[-\phi_y, \phi_x]}{|\nabla\phi|} \\
 \kappa &= \operatorname{div}\left(\frac{\nabla\phi}{|\nabla\phi|}\right)
 \end{aligned} \tag{28}$$

$$\begin{aligned}
 \vec{V}_s &= [u_s, v_s] = [\langle\nabla u, \vec{t}\rangle, \langle\nabla v, \vec{t}\rangle] \\
 \operatorname{sign}(\langle\vec{V}, \vec{n}\rangle) &= \operatorname{sign}(\langle\vec{V}, \nabla\phi\rangle).
 \end{aligned}$$

Thereby, the explicit curve evolution as a gradient descent flow for $\rho(\alpha) = |\alpha|$ is given by

$$C_t = \operatorname{sign}(\langle\vec{V}, \vec{n}\rangle)\Delta I\vec{n}, \tag{29}$$

for which the implicit level set evolution is given by

$$\phi_t = \text{sign}(\langle \vec{V}, \nabla \phi \rangle) \Delta I |\nabla \phi|. \quad (30)$$

In the more general case, in which ρ is an arbitrary function, we use the above relations in the level set evolution equation to obtain:

$$\begin{aligned} \phi_t = & \left[-\kappa \rho + \left(\text{div}(\vec{V}) + \left\langle \vec{V}, \frac{\nabla \phi}{|\nabla \phi|} \right\rangle \kappa \right) \rho' \right. \\ & + \left(\left\langle \vec{V}_s, \frac{\nabla \phi}{|\nabla \phi|} \right\rangle \left\langle \vec{V}, \frac{\bar{\nabla} \phi}{|\nabla \phi|} \right\rangle \right. \\ & \left. \left. - \kappa \left\langle \vec{V}, \frac{\bar{\nabla} \phi}{|\nabla \phi|} \right\rangle^2 \right) \rho'' \right] |\nabla \phi| \end{aligned} \quad (31)$$

Vasilevskiy and Siddiqi independently came up with the $\phi_t = \text{div}(\vec{V})|\nabla \phi|$ equation for active contours (Vasilevskiy and Siddiqi, 2001) as a result of a geometric alignment integral measure. However, they did not notice the direct link to the Marr-Hildreth edge detector, and their operator is not invariant to inverse contrast, as their $\rho(\alpha) = \alpha$ (which we used in our over simplistic examples) is not symmetric. For inverse contrast invariance of the process we require ρ to be symmetric, that is $\rho(\alpha) = \rho(-\alpha)$.

Finally, the explicit curve evolution as a gradient descent flow for Eq. (10) is given by

$$C_t = \text{sign}(\langle \vec{v}, \vec{\xi} \rangle) (\Delta I - I_{\eta\eta}) \vec{n},$$

for which the implicit level set evolution is given by

$$\phi_t = \text{sign}(\langle \vec{v}, \vec{\xi} \rangle) (\Delta I - I_{\eta\eta}) |\nabla \phi|.$$

We can now add to our model the geodesic active contour term of Caselles et al. (1997), the thresholding term, or its version with dynamic expectation defined by the minimal variance criterion of Chan and Vese (1999). The functional now takes the form

$$\arg \max_{c_1, c_2, C} \psi(C, c_1, c_2),$$

for

$$\begin{aligned} \psi(C, c_1, c_2) = & \oint \text{sign}(\langle \vec{v}, \vec{\xi} \rangle) \langle \nabla I, \vec{n} \rangle ds \\ & - \iint_{\Omega_C} \text{sign}(\langle \vec{v}, \vec{\xi} \rangle) I_{\eta\eta} dx dy \\ & - \alpha \left(\iint_{\Omega_C} (I - c_1)^2 dx dy \right. \end{aligned}$$

$$\begin{aligned} & \left. + \iint_{\Omega \setminus \Omega_C} (I - c_2)^2 dx dy \right) \\ & - \epsilon \oint g(C(s)) ds, \end{aligned}$$

where g is an edge indicator function given for example by $g(x, y) = 1/(1 + |\nabla I|^2)$, and $C = \partial \Omega_C$. The Euler Lagrange equations as a gradient descent in level set formulation are given by

$$\begin{aligned} \phi_t = & \left(\text{sign}(\langle \vec{v}, \vec{\xi} \rangle) I_{\xi\xi} + 2\alpha(c_2 - c_1) \left(I - \frac{c_1 + c_2}{2} \right) \right. \\ & \left. + \epsilon \text{div} \left(g(x, y) \frac{|\nabla \phi|}{|\nabla \phi|} \right) \right) |\nabla \phi|. \end{aligned}$$

$$c_1 = \frac{1}{|\Omega_C|} \iint_{\Omega_C} I(x, y) dx dy$$

$$c_2 = \frac{1}{|\Omega \setminus \Omega_C|} \iint_{\Omega \setminus \Omega_C} I(x, y) dx dy,$$

where $|\Omega_C|$ denotes the area of the regions Ω_C .

Efficient solutions for these equation can use multiplicative or additive implicit numerical schemes based on alternating dirrections, as the AOS (Lu et al., 1991, 1992; Weickert et al., 1998), LOD (Kimmel, 2003, to appear), or ADI methods, coupled with a narrow band approach (Chopp, 1993; Adalsteinsson and Sethian, 1995). These ideas were first adopted to solve the geodesic active contour model in Goldenberg et al. (2001). See (Kimmel, to appear, 2002) for a Matlab code.

4. Open Active Contours for Optimal Edge Integration

4.1. The Fua-Leclerc Geometric Model

Fua and Leclerc (1990), were first to propose a geometric model for motion of open curves in the image-plane to optimize an “edge” finding functional. We shall first describe the Fua-Leclerc functional and then replace the “geodesic active contour” part of it with our new edge integration quality measure. Let

$$L(C) = \int_0^1 |C_p| dp, \quad (32)$$

be the arclength of an open curve $C(p)$. Adding the variation $\eta(p)$ to the curve, such that $\tilde{C}(p) = C(p) + \epsilon \eta(p)$, differentiating w.r.t. ϵ , and letting ϵ go to zero,

yields

$$L'(C) = - \int_0^L \kappa \langle \vec{n}, \eta \rangle ds + \langle \eta(L), \vec{t}(L) \rangle - \langle \eta(0), \vec{t}(0) \rangle, \quad (33)$$

where s is the arclength parameter (see Appendix for derivation). Also, following Fua and Leclerc, consider

$$L_g(C) = \int_0^L g(C(s)) ds, \quad (34)$$

where g is some suitably defined “edge indicator” function, for example $g(x, y) = 1/(|\nabla I|^2 + 1)$. The first variation of $L_g(C)$ can be easily shown to be given by

$$\begin{aligned} L'_g(C) &= \int_0^L (\langle \nabla g, \vec{n} \rangle - \kappa g) \langle \vec{n}, \eta \rangle ds \\ &\quad + g(C(L)) \langle \eta(L), \vec{t}(L) \rangle \\ &\quad - g(C(0)) \langle \eta(0), \vec{t}(0) \rangle. \end{aligned} \quad (35)$$

(See Appendix for a full derivation).

The Fua-Leclerc functional is defined as

$$\psi_g(C) = \frac{L_g(C)}{L(C)}. \quad (36)$$

Computing the first variation, we have that

$$\frac{\delta \psi_g}{\delta C} = \frac{LL'_g - L'L_g}{L^2} = 0, \quad (37)$$

should hold for any η . Therefore, the following conditions must be satisfied,

$$LL'_g = L'L_g, \quad (38)$$

or explicitly,

$$\begin{aligned} L \cdot &\left(\int_0^L (\langle \nabla g, \vec{n} \rangle - \kappa g) \vec{n} \eta ds + \eta(L)g(C(L))\vec{t}(L) \right. \\ &\quad \left. - \eta(0)g(C(0))\vec{t}(0) \right) \\ &= L_g \cdot \left(\int_0^L -\kappa \vec{n} \eta ds + \eta(L)\vec{t}(L) - \eta(0)\vec{t}(0) \right). \end{aligned} \quad (39)$$

Thus, we should verify the following necessary conditions for a local extremum to hold for any η ,

$$\begin{aligned} \int_0^L (L(\langle \nabla g, \vec{n} \rangle - \kappa g) + L_g \kappa) \langle \vec{n}, \eta \rangle ds &= 0 \\ L\eta(L)g(C(L))\vec{t}(L) &= L_g \langle \eta(L), \vec{t}(L) \rangle \\ L\eta(0)g(C(0))\vec{t}(0) &= L_g \langle \eta(0), \vec{t}(0) \rangle. \end{aligned} \quad (40)$$

Therefore, the geometric conditions that must be met along the curve and at its end points, are:

$$\begin{aligned} \left(\left(\frac{L_g}{L} - g \right) \kappa + \langle \nabla g, \vec{n} \rangle \right) \vec{n} &= 0 \\ g(C(0)) &= \frac{L_g}{L} \\ g(C(L)) &= \frac{L_g}{L}. \end{aligned} \quad (41)$$

We can use these conditions to guide a gradient descent process for an active contour evolution toward the local minimum of the Fua-Leclerc functional. To do that we apply the following evolution equation along the curve and at its end points,

$$C_t = \left(\kappa g - \langle \nabla g, \vec{n} \rangle - \frac{L_g}{L} \kappa \right) \vec{n}. \quad (42)$$

The first two terms depict the geodesic active contour (Caselles et al., 1997) model, while the third term directs the curve to gain length by applying the inverse geometric heat equation at points where $g(C(s)) < L_g/L$. We still need to design the motion of the end points. Consider the end point $C(L)$. The curve should reduce its length if $g(C(L)) > L_g/L$, in which case the end point should move along the tangent $-\vec{t}(L)$. Hence, for example, we can use the following evolution rules at the end points:

$$\begin{aligned} C_t(0) &= (Lg(C(0)) - L_g)\vec{t}(0) \\ C_t(L) &= (L_g - Lg(C(L)))\vec{t}(L). \end{aligned} \quad (43)$$

4.2. Our Optimal Edge Integration

We propose to use our measure, $L_\rho = \int \rho(\alpha) ds$ instead of L_g , in the Fua-Leclerc functional. Here we compute the evolution equations that propagate the

open curve C towards a maximum of the functional

$$\psi_\rho(C) = \frac{L_\rho}{L}. \quad (44)$$

Therefore, we are searching for $\arg_C \max \psi_\rho(C)$. The quantity L in this *maximization* process, penalizes the length of the curve, i.e. it plays a role opposite from its role in the *minimization* of the Fua-Leclerc functional.

We now use the $\delta\psi_\rho/\delta C$ expression developed in the previous sections for the general $\rho(\langle \vec{V}, \vec{n} \rangle)$ closed curve case. We have that

$$L'_\rho(C) = \int_0^L \eta \cdot \frac{\delta\psi_\rho}{\delta C} ds + \eta \cdot (\rho\vec{t} - \rho'\langle \vec{V}, \vec{t} \rangle \vec{n})|_0^L. \quad (45)$$

Using these conditions in the Fua-Leclerc formulae yield along the curve,

$$L \frac{\delta\psi_\rho}{\delta C} + L_\rho \kappa \vec{n} = 0, \quad (46)$$

and

$$L(\rho\vec{t} - \rho'\langle \vec{V}, \vec{t} \rangle \vec{n}) = L_\rho \vec{t}, \quad (47)$$

at the end points $C(L)$ and $C(0)$. For $\rho(\alpha) = |\alpha|$, the gradient descent flow along the curve is given by

$$\begin{aligned} C_t &= \text{sign}(\langle \nabla I, \vec{n} \rangle) \Delta I \vec{n} + \frac{L_\rho}{L} \kappa \vec{n} \\ C_t(0) &= (L_\rho - L_\rho) \vec{t} - \rho'\langle \vec{V}, \vec{t} \rangle \vec{n} \\ C_t(L) &= (L_\rho - L_\rho) \vec{t} + \rho'\langle \vec{V}, \vec{t} \rangle \vec{n}. \end{aligned} \quad (48)$$

4.3. A Simpler Formulation for the New Optimal Edge Integration

Functionals that involve ratio of two integral measures, like the Fua-Leclerc functional, require integration along the contours for a proper gradient descent flow. Integral parts are present in the EL equations which require computationally intensive global integration procedures for the computation of the proper flow. Recall however that our goal is to maximize $\psi_\rho(C)$ on one hand, that leads to long curves, while also penalizing the length of the curve on the other hand. We shall therefore consider the following alternative functional that would also realize these goals,

$$\tilde{\psi}_\rho(C) = L_\rho - L. \quad (49)$$

The EL equations in this case are given by

$$0 = \frac{\delta\tilde{\psi}_\rho(C)}{\delta C} + \kappa \vec{n}, \quad (50)$$

along the curve, and

$$0 = (\rho - 1)\vec{t} - \rho'\langle \vec{V}, \vec{t} \rangle \vec{n}, \quad (51)$$

at the end points. The motivation for the tangential term at the end point is obvious, it either extends or shrinks the curve. The normal term pulls it from running parallel to the vector field and directs the end point towards the center of the edge (where ρ' should be zero). These two components define the motion at the end points. For $\rho(\alpha) = |\alpha|$ and $\vec{V} = \nabla I$ we have

$$\begin{aligned} C_t &= \text{sign}(\langle \nabla I, \vec{n} \rangle) \Delta I \vec{n} + \kappa \vec{n} \\ C_t(0) &= (|\langle \nabla I, \vec{n} \rangle| - 1)\vec{t} - \text{sign}(\langle \nabla I, \vec{n} \rangle) \langle \nabla I, \vec{t} \rangle \vec{n} \\ C_t(L) &= (1 - |\langle \nabla I, \vec{n} \rangle|)\vec{t} + \text{sign}(\langle \nabla I, \vec{n} \rangle) \langle \nabla I, \vec{t} \rangle \vec{n}. \end{aligned} \quad (52)$$

5. Simulation Results

Most of the figures are in color that would appear only in the electronic version of the paper. Figure 4 compares the more robust edge detector given by the zero crossings of $I_{\xi\xi}$, and the zero crossings of the Laplacian. It is obvious that $I_{\xi\xi}$ is less sensitive to the noise.

Next, we compared between edge integration results of the Haralick-like and the Laplacian terms within the geometric active contour model. Comparing the results of the two methods clearly demonstrates the regularization effect of the Haralick-like term. While the Laplacian term causes the contour to oscillate and capture insignificant and small structures, the Haralick-like term regularizes the propagating curve and leads to smoother boundary curves. In all the ‘‘closed contour’’ cases we started from the image border as the initial contour, and applied a multi-resolution coarse to fine procedure, as in Paragios and Deriche (2000), to speed up the segmentation process.

Next, we tested the edge integration methods discussed in this paper on two simple examples, see Fig. 5. The first presented segmentation examples shown are not typical for active contours and

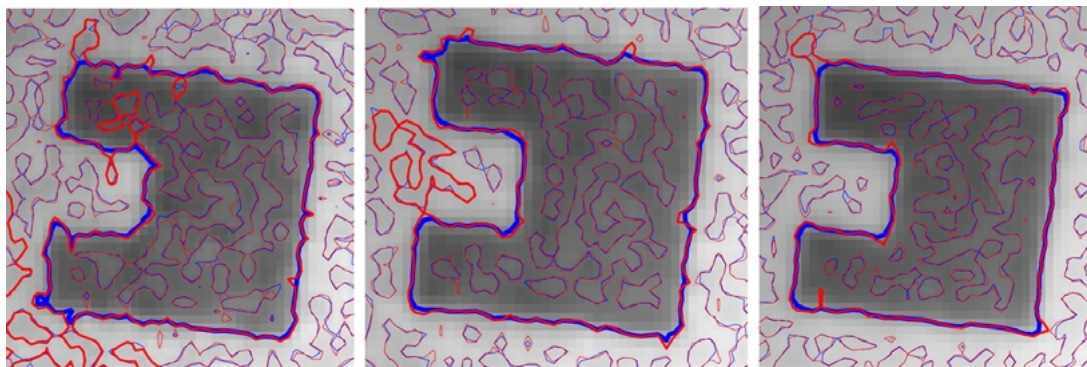


Figure 4. Zero crossings of $I_{\xi\xi}$, in blue, compared to zero crossings of ΔI , in red, for edge detection of an object with various noise levels.

could also be processed with less sophisticated methods. However, they clearly exhibit the difficulties of existing active contour models and are therefore quite useful for comparison of the different methods.

The additional GAC term for regularization and the multi-resolution both play an important factor in propagating the contour in homogeneous or noisy regions where the alignment in term of the image Laplacian is meaningless. However, the alignment plays a crucial role for final fine localization of the boundary edges.

Figure 6 shows the advantage of the Laplacian model in cases where only the gradient is affected, the Laplacian being invariant to an additive intensity

plane, as well as in cases where the Laplacian is also changed by a constant when a parabola was added to the intensity surface. Figures 7 and 8 clearly exhibit the segmentation advantages of the Laplacian active curve model as a core with the geodesic active term used as a regularization. We here used the functional

$$\psi(C) = \oint_C \rho(\alpha) ds - \beta \oint_C g(C(s)) ds \quad (53)$$

where β is a small positive constant, $\rho(\alpha) = |\alpha|$, and $\alpha = \langle \nabla I, \vec{n} \rangle$. g is an edge indicator function with lower values along the edges. In this case, the

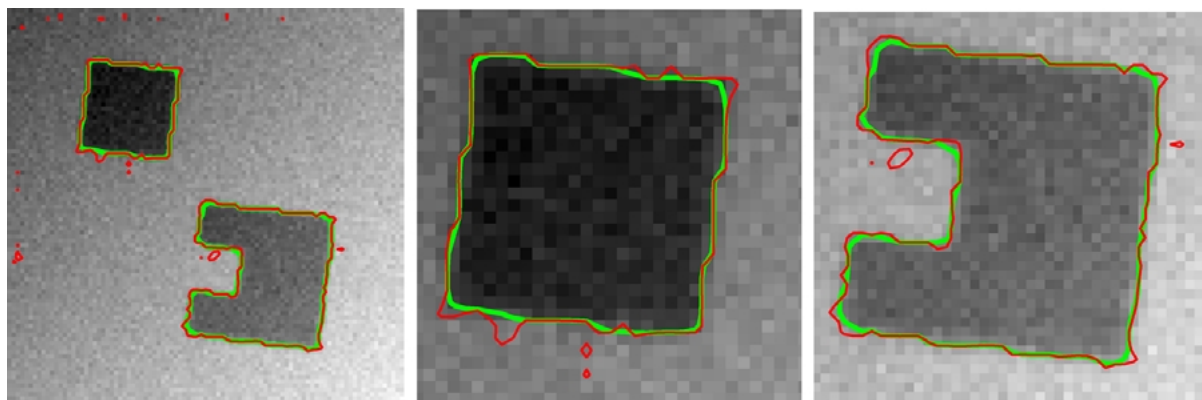


Figure 5. Synthetic images with a tilted intensity plane added to the original image and additive Gaussian noise. The edge integration via geometric active contour results for both the Laplacian term (in red) and the second order derivative along the gradient direction Haralick-like term (in green) are shown in two resolutions.

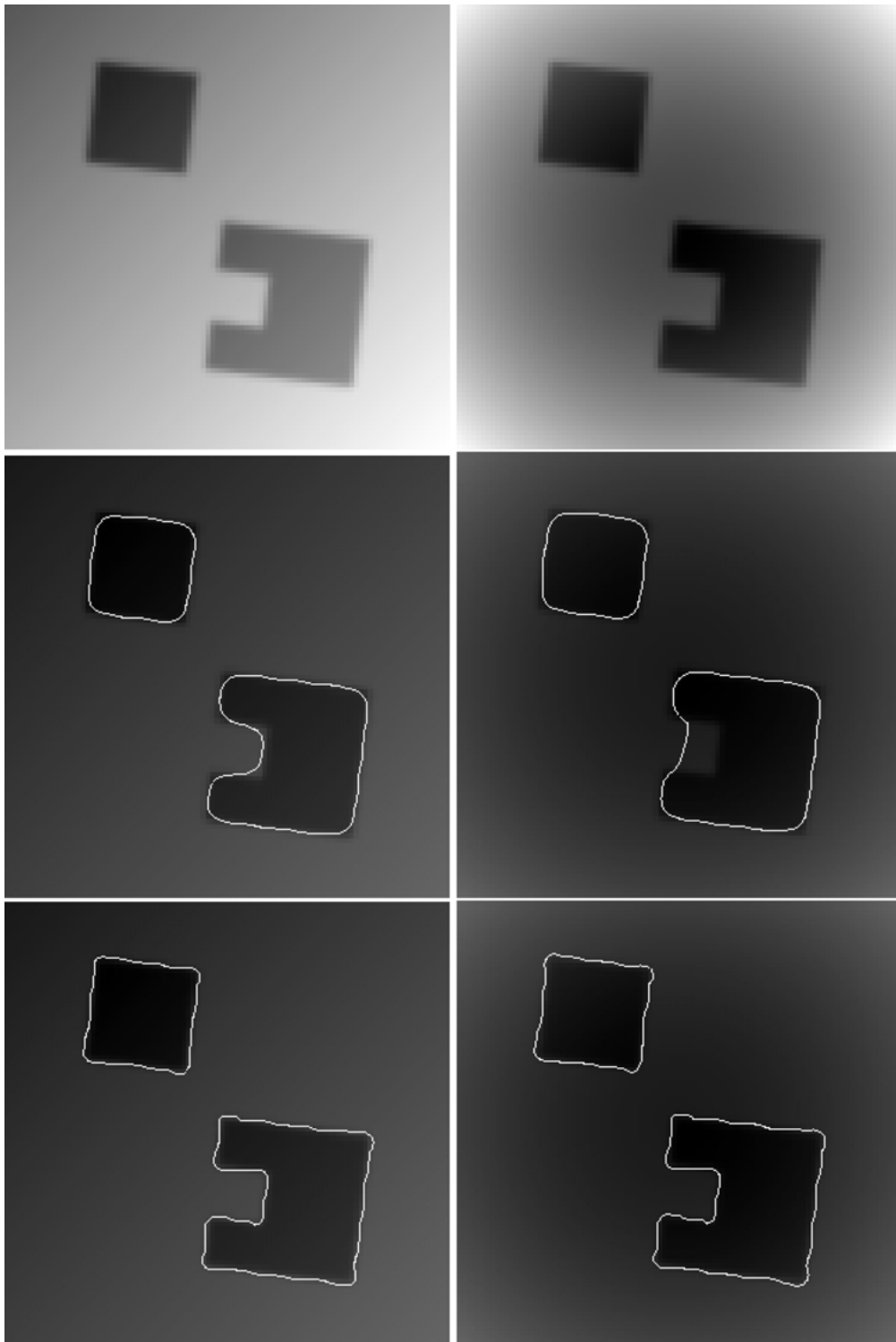


Figure 6. Top: Synthetic images with a tilted intensity plane added to the original image on the left, and a parabola intensity surface added to the original image on the right. Middle row: Segmentation results with the GAC model given by $\phi_t = \text{div}(g(x, y) \frac{\nabla \phi}{|\nabla \phi|}) |\nabla \phi|$. Bottom: Segmentation results with the Laplacian model in Eq. (30).

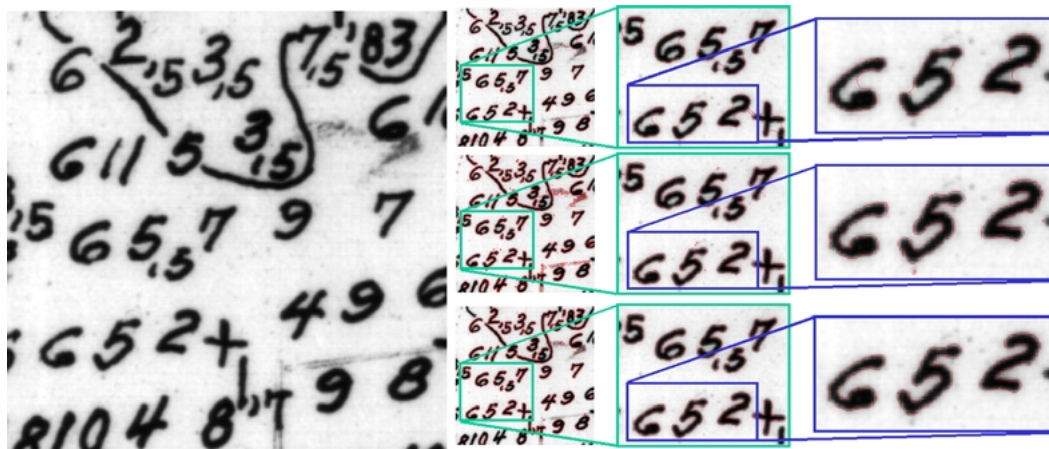


Figure 7. Left: Map input image. Right: The active contours results, in which the upper row shows the geodesic active contour results, middle row presents the results of the Laplacian active contour, and bottom row is a combination of the two.

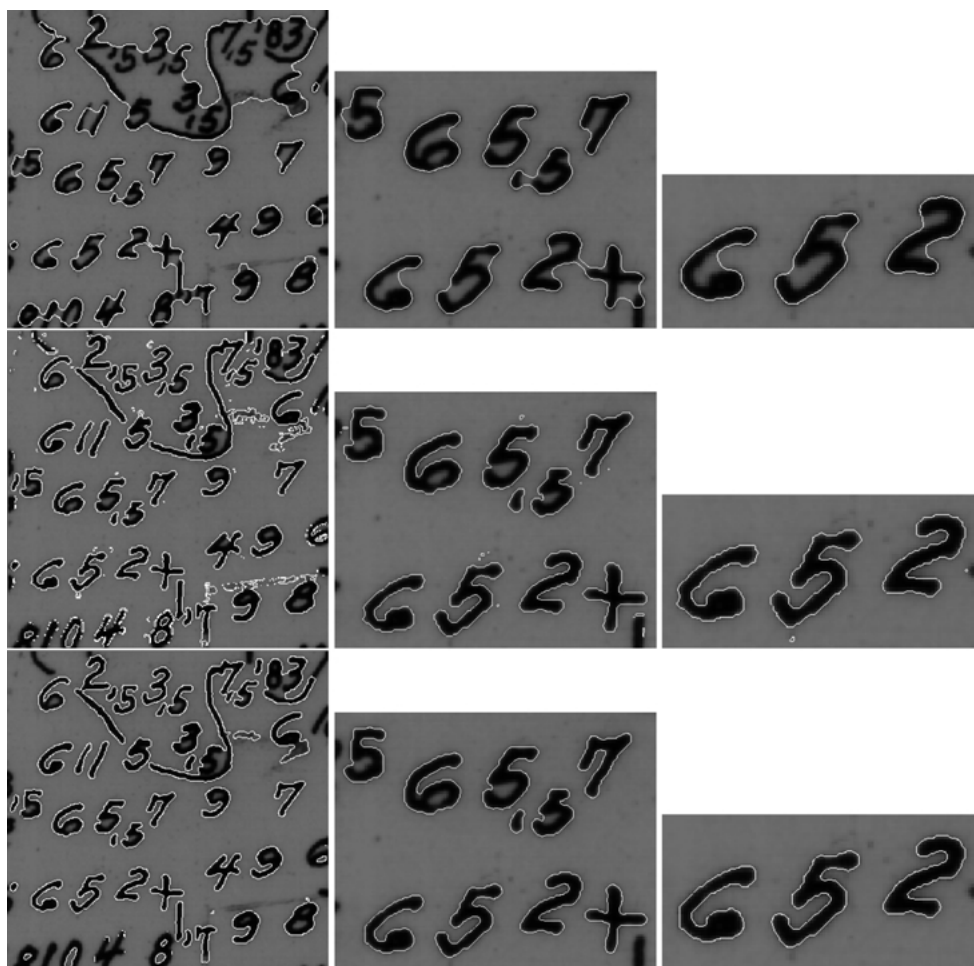


Figure 8. Top: Geodesic active contour results. Middle: Laplacian active contours. Bottom: Using the geodesic active contours as a regularization for the Laplacian active contour.

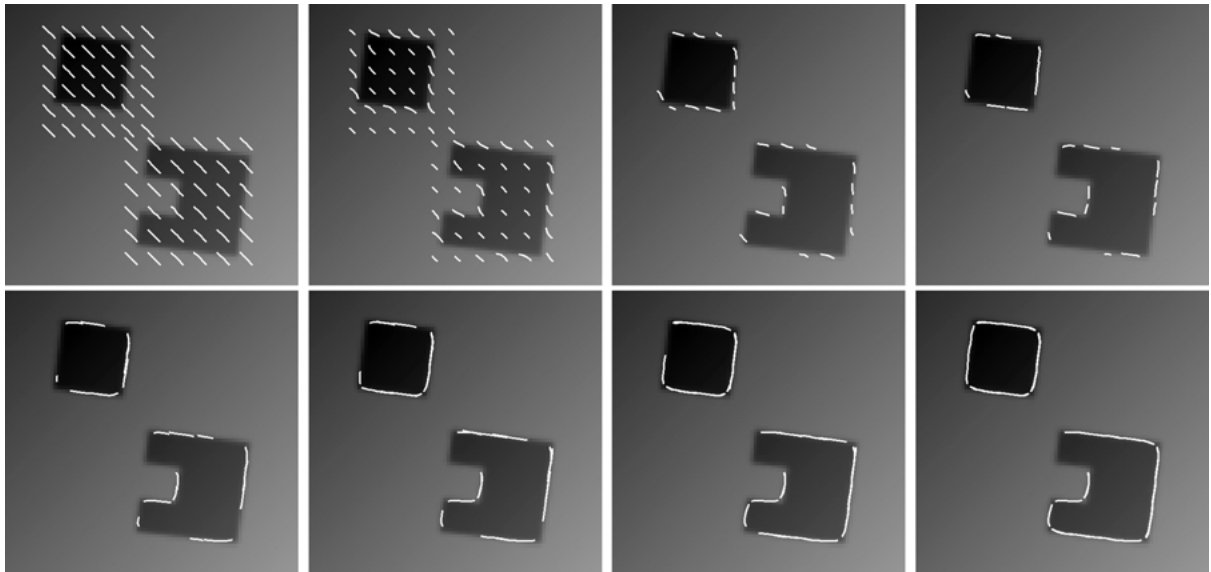


Figure 9. Open geometric Laplacian active contours: The initial small diagonal lines (top left frame) deform and either shrink and vanish or extend along the boundaries of the objects and capture their shapes (the evolution sequence is top to bottom left to right).

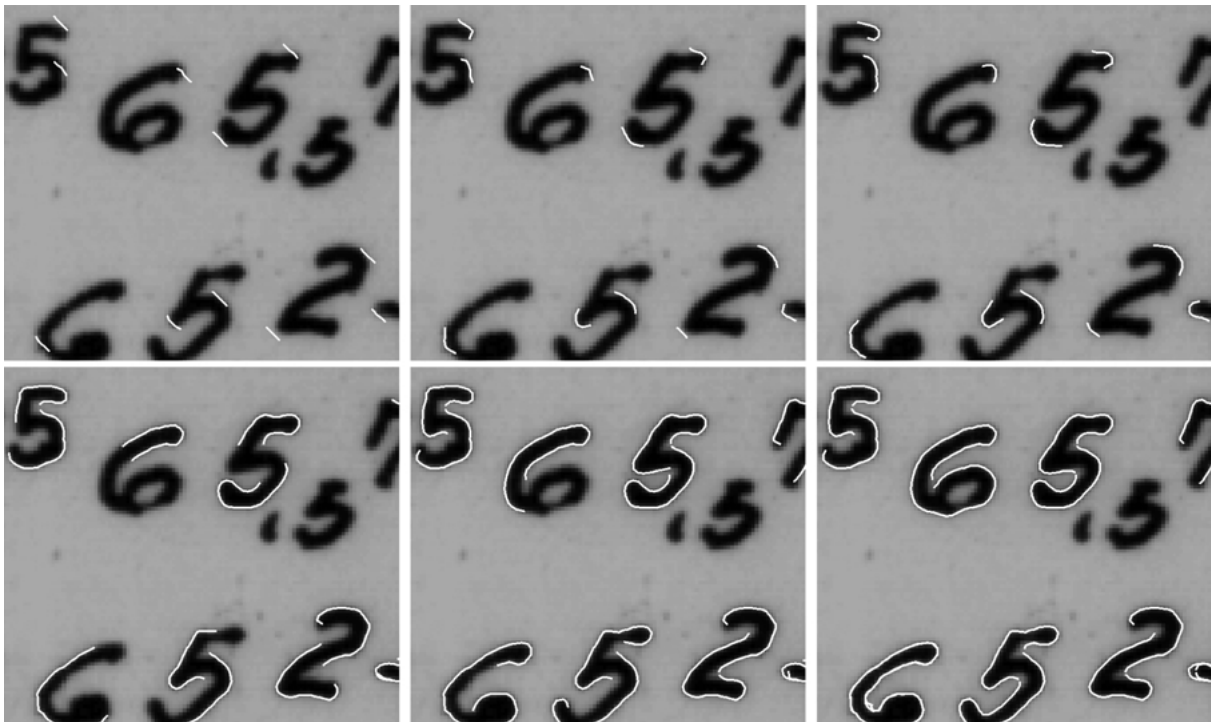


Figure 10. Open geometric Laplacian active contours: The small curves (top left frame) extend along the boundaries and capture most of the outer contours of the text symbols (the evolution sequence is top to bottom left to right).

gradient descent flow for maximizing $\psi(C)$ is given by

$$C_t = (\text{sign}(\langle \nabla I, \vec{n} \rangle) \Delta I + \beta(g\kappa - \langle \nabla g, \vec{n} \rangle) \vec{n}). \quad (54)$$

The level set formulation for this flow is

$$\phi_t = \left(\text{sign}(\langle \nabla I, \nabla \phi \rangle) \Delta I + \beta \text{div} \left(g_1 \frac{\nabla \phi}{|\nabla \phi|} \right) \right) |\nabla \phi|. \quad (55)$$



Figure 11. Open geometric Laplacian active contours: Left to right is the evolution process of a set of initial contours shown at the left frame.

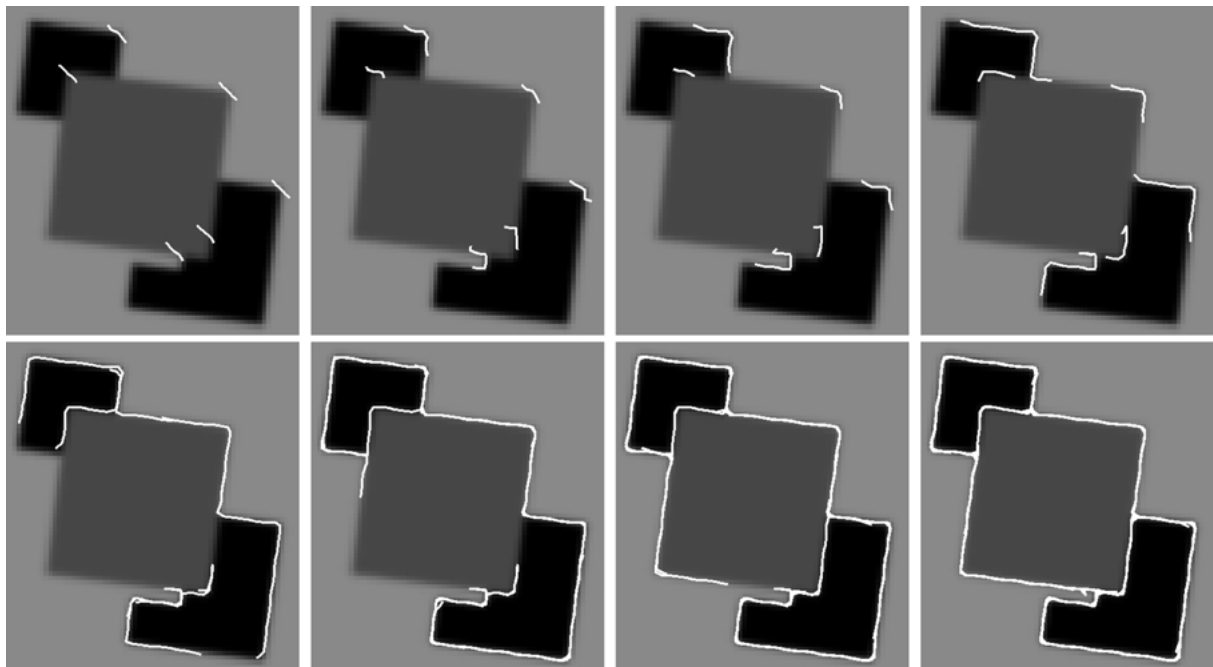


Figure 12. Open geometric Laplacian active contours: Left to right, top to bottom, is the evolution process of a set of initial contours shown at the top left.

For implementation considerations we used upwind schemes for most terms, and central difference approximation only for the diffusive GAC term $g \operatorname{div}(\frac{\nabla \phi}{|\nabla \phi|})|\nabla \phi|$.

Next, we applied our open contour model for edge integration on similar images, but here we started with short contour segments that expanded and locked onto boundaries, if such existed in the vicinity of the initialized contours. If no boundaries are detected locally, the contour segments shrink and eventually disappear. The numerical implementation for the open contour case is an explicit “marker-points” based model which was easier to program in this case. One could also use a level set defined in a band around the active contour with explicit motion of the end points. At each iteration the marker-points are re-distributed along the contour to form equi-distant numerical representations of the contour. A simple monitoring procedure, removes a marker point when successive marker points get too close to one another, and adds a new marker point in the middle of two successive marker points when the distance between them gets larger than a given threshold. The examples show how initial segments expand and deform until they lock onto the boundaries of rather complex shapes. Figures 9–12 demonstrate the application of the scheme to edge integration in a bit less trivial scenarios. The same set parameters were used for all examples.

6. Conclusions

In this paper we proposed to incorporate the directional information that is generally ignored when designing edge integration methods in a variational framework. Simulations that were performed with the newly defined edge integration processes demonstrated their excellent performance as compared to the best existing edge integration methods. Our extended active contour models are just a few examples of the many possible combinations of geometric measures. Other functionals that could be considered to either open or closed curves are $L_\rho - L_g$, or $\int \rho(\alpha)q(|\nabla I|)ds$, for an edge indicator function like $q = 1 - g(|\nabla I|)$ or $q(|\nabla I|) = \sqrt{|\nabla I|^2 + 1}$. For closed curves, the ψ_ρ part is most effective when the curve is close to its final location, therefore, the

functional $\oint[\rho(\alpha)(1 - g) - g]ds$ could also be considered. Efficient numerical methods can be applied to solve the resulting geometric flows. We believe that better understanding via integral measures of successful low level vision operators, could lead to better ones. These improved operators could then be coupled together into more general schemes, similar to the way we incorporated the Haralick/Canny edge detector into our variational edge integration processes.

Appendix

Let

$$L(C) = \int_0^1 |C_p| dp, \quad (56)$$

be the arclength of an open curve $C(p)$. We add the variation $\eta(p)$ to the curve, such that $\tilde{C}(p) = C(p) + \epsilon\eta(p)$. Next, differentiating w.r.t. ϵ , and letting ϵ go to zero, we have

$$\begin{aligned} L'(C) &= \frac{\delta L}{\delta C} = \lim_{\epsilon \rightarrow 0} \frac{d}{d\epsilon} \int_0^1 \langle \tilde{C}_p, \tilde{C}_p \rangle^{1/2} dp \\ &= \lim_{\epsilon \rightarrow 0} \int_0^1 |\tilde{C}_p|^{-1} \langle \eta_p, \tilde{C}_p \rangle dp \\ &= \int_0^1 \langle \eta_p, \vec{t} \rangle dp \\ &= \langle \eta, \vec{t} \rangle \Big|_0^1 - \int_0^1 \left\langle \eta, \frac{d}{dp} \vec{t} \right\rangle dp \\ &= \langle \eta(1), \vec{t}(1) \rangle - \langle \eta(0), \vec{t}(0) \rangle \\ &\quad - \int_0^1 \langle \kappa \eta, \vec{n} \rangle |C_p| dp \\ &= - \int_0^L \kappa \langle \vec{n}, \hat{\eta} \rangle ds + \langle \hat{\eta}(L), \vec{t}(L) \rangle \\ &\quad - \langle \hat{\eta}(0), \vec{t}(0) \rangle, \end{aligned} \quad (57)$$

where s is the arclength parameter and $\hat{\eta}(s(p)) = \eta(p)$, for $ds = |C_p| dp$. Which proves the result given by Eq. (33).

In a similar way Eq. (35) is derived by

$$\begin{aligned}
L'_g(C) &= \lim_{\epsilon \rightarrow 0} \frac{d}{d\epsilon} \int_0^1 g(\tilde{C}(p)) \langle \tilde{C}_p, \tilde{C}_p \rangle^{1/2} dp \\
&= \int_0^L \langle \nabla g, \hat{\eta} \rangle ds + \int_0^1 g(\eta_p, \vec{t}) dp \\
&= \int_0^L (\langle \nabla g, \vec{n} \rangle \langle \hat{\eta}, \vec{n} \rangle + \langle \nabla g, \vec{t} \rangle \langle \hat{\eta}, \vec{t} \rangle) ds \\
&\quad + g(\eta, \vec{t}) \Big|_0^1 - \int_0^1 \left\langle \eta, \frac{d}{dp}(g\vec{t}) \right\rangle dp \\
&= g(\hat{\eta}, \vec{t}) \Big|_0^L + \int_0^L (\langle \nabla g, \vec{n} \rangle \langle \hat{\eta}, \vec{n} \rangle \\
&\quad + \langle \nabla g, \vec{t} \rangle \langle \hat{\eta}, \vec{t} \rangle) ds \\
&\quad - \int_0^1 \langle \nabla g, \vec{t} \rangle \langle \eta, \vec{t} \rangle |C_p| dp \\
&\quad - \int_0^1 g \langle \eta, \kappa \vec{n} \rangle |C_p| dp \\
&= \int_0^L (\langle \nabla g, \vec{n} \rangle - \kappa g) \langle \vec{n}, \hat{\eta} \rangle ds \\
&\quad + g(C(L)) \langle \hat{\eta}(L), \vec{t}(L) \rangle - g(C(0)) \langle \hat{\eta}(0), \vec{t}(0) \rangle.
\end{aligned} \tag{58}$$

Acknowledgments

We thank our students Evgeni Krimer and Roman Barsky for implementing the first version of the open active contours models, and the IJCV reviewers for their detailed comments that help us improve the presentation of the paper. This research is supported in part by a grant from the ISF (Israeli Science Foundation), administered by the Israeli Academy of Science.

References

- Adalsteinsson, D. and Sethian, J.A. 1995. A fast level set method for propagating interfaces. *J. of Comp. Phys.*, 118:269–277.
- Canny, J. 1986. A computational approach to edge detection. *IEEE Trans. on PAMI*, 8(6):679–698.
- Caselles, V., Catta, F., Coll, T., and Dibos, F. 1993. A geometric model for active contours. *Numerische Mathematik*, 66:1–31.
- Caselles, V., Kimmel, R., and Sapiro, G. 1997. Geodesic active contours. *International Journal of Computer Vision*, 22(1):61–79.
- Chan, T. and Vese, L. 1999. An active contour model without edges. In *Scale-Space Theories in Computer Vision*, pp. 141–151.

- Chopp, D.L. 1993. Computing minimal surfaces via level set curvature flow. *J. of Computational Physics*, 106(1):77–91.
- Deriche, R. 1987. Using Canny's criteria to derive a recursively implemented optimal edge detector. *International Journal of Computer Vision*, 1:167–187.
- Evans, L. and Garipey, R. 1992. *Measure Theory and Fine Properties of Functions*. CRC Press.
- Fua, P. and Leclerc, Y.G. 1990. Model driven edge detection. *Machine Vision and Applications*, 3:45–56.
- Goldenberg, R., Kimmel, R., Rivlin, E., and Rudzsky, M. 2001. Fast geodesic active contours. *IEEE Trans. on Image Processing*, 10(10):1467–1475.
- Haralick, R. 1984. Digital step edges from zero crossing of second directional derivatives. *IEEE Trans. on Pattern Analysis and Machine Intelligence*, 6(1):58–68.
- Kass, M., Witkin, A., and Terzopoulos, D. 1988. Snakes: Active contour models. *International Journal of Computer Vision*, 1:321–331.
- Kimmel, R. 2003. Fast edge integration. In *Level Set Methods and Their Applications in Computer Vision*, Chapter 3. Springer Verlag: NY.
- Kimmel, R. to appear. *Numerical Geometry of Images*. Springer: Boston, NY.
- Kimmel, R. and Bruckstein, A.M. 2001. Regularized Laplacian zero crossings as optimal edge integrators. In *Proceedings of Image and Vision Computing, IVCNZ01*, New Zealand.
- Kimmel, R. and Bruckstein, A.M. 2002. On edge detection edge integration and geometric active contours. In *Proceedings of Int. Symposium on Mathematical Morphology, ISMM2002*, Sydney, New South Wales, Australia.
- Lu, T., Neittaanmaki, P., and Tai, X-C. 1991. A parallel splitting up method and its application to Navier-Stokes equations. *Applied Mathematics Letters*, 4(2):25–29.
- Lu, T., Neittaanmaki, P., and Tai, X-C. 1992. A parallel splitting up method for partial differential equations and its application to Navier-Stokes equations. *RAIRO Math. Model. and Numer. Anal.*, 26(6):673–708.
- Malladi, R., Sethian, J.A., and Vemuri, B.C. 1993. A topology-independent shape modeling scheme. In *SPIE's Geometric Methods in Computer Vision II*, vol. SPIE 2031, pp. 246–255.
- Malladi, R., Sethian, J.A., and Vemuri, B.C. 1995. Shape modeling with front propagation: A level set approach. *IEEE Trans. on PAMI*, 17:158–175.
- Marr, D. 1982. *Vision*. Freeman: San Francisco.
- Marr, D. and Hildreth, E. 1980. Theory of edge detection. In *Proc. of the Royal Society London B*, 207:187–217.
- Osher, S.J. and Sethian, J.A. 1988. Fronts propagating with curvature dependent speed: Algorithms based on Hamilton-Jacobi formulations. *J. of Comp. Phys.*, 79:12–49.
- Paragios, N. and Deriche, R. 2000. Geodesic active contours and level sets for the detection and tracking of moving objects. *IEEE Trans. on PAMI*, 22(3):266–280.
- Paragios, N.K., Mellina-Gotardo, O., and Ramesh, V. 2001. Gradient vector flow fast geodesic active contours. In *Proceedings ICCV'01*, Vancouver, Canada.
- Sethian, J.A. 1996. *Level Set Methods: Evolving Interfaces in Geometry, Fluid Mechanics, Computer Vision and Materials Sciences*. Cambridge University Press.

- Vasilevskiy, A. and Siddiqi, K. 2001. Flux maximizing geometric flows. In *Proceedings Int. Conf. on Computer Vision*, Vancouver, Canada.
- Weickert, J., ter Haar Romeny, B.M., and Viergever, M.A. 1998. Efficient and reliable scheme for nonlinear diffusion filtering. *IEEE Trans. on Image Processing*, 7(3):398–410.
- Xu, C. and Prince, J.L. 1998. Snakes, shapes, and gradient vector flow. *IEEE Trans. on Image Processing*, 7(3):359–369.
- Zhu, S., Lee, T., and Yuille, A. 1995. Region competition: Unifying snakes, region growing, energy/bayes/mdl for multi-band image segmentation. In *Proc. ICCV'95*, Cambridge, pp. 416–423.